

High-Pressure Experimental Data of CO₂ + Mitotane and CO₂ + Ethanol + Mitotane Mixtures

W. M. Giufrida,[†] S. B. Rodriguez-Reartes,[‡] C. G. Alonso,[†] M. S. Zabaloy,[‡] V. F. Cabral,[†] F. W. Tavares,^{*,§} and L. Cardozo-Filho[†]

[†]Departamento de Engenharia Química, Universidade Estadual de Maringá, Av. Colombo, 5790, Bloco D-90, 87020-900, Maringá, PR, Brazil

[‡]Planta Piloto de Ingeniería Química, Universidad Nacional del Sur, CONICET, CC 717, 8000 Bahía Blanca, Argentina

[§]Escola de Química and Programa de Engenharia Química/COPPE, Universidade Federal do Rio de Janeiro, Cidade Universitária, Ilha do Fundão, 21949-900, Rio de Janeiro, RJ, Brazil

ABSTRACT: This work presents new experimental phase equilibrium data for mitotane in supercritical CO₂ and mitone in supercritical CO₂ plus ethanol. The synthetic-static method in a high-pressure variable-volume view cell was used to measure the solid–fluid (SF) and the fluid–fluid (FF) equilibrium data. The phase equilibrium experiments were carried out in the temperature range from (298 to 333) K and in the pressure range from (3.44 to 21.84) MPa. The Peng–Robinson equation of state (PR-EoS) was used for describing the fluid phases, and an expression for the fugacity of pure solid mitotane was used for representing the solid phase. This made it possible to model the SF and FF equilibrium data for the CO₂ + mitotane mixtures. Fair agreement was found between experimental and calculated values.

1. INTRODUCTION

Mitotane ((*R,S*)-1-chloro-2-[2,2-dichloro-1-(4-chlorophenyl)-ethyl]-benzene) is a chiral drug used in the treatment of adrenocortical carcinoma. Nowadays, such drug is marketed as a racemic mixture of their R and S enantiomers. However, in most cases of chiral drugs, each isolated enantiomer presents different pharmacological effects and toxicological profiles, and thus they must be tested separately.

In two recent articles,^{1,2} Santana and his colleagues used a combination of supercritical fluid chromatography (SFC) with the simulated moving bed (SMB) technique for the enantioseparation of mitotane. In the second paper,² the authors separated the enantiomers of mitotane using a Kromasil CHI-TBB column and four different carrier gases (mobile phase), that is, pure CO₂, CO₂ + methanol, CO₂ + ethanol, and CO₂ + isopropanol. The range for the concentration of alcohol in the mobile phase was from (2.6 to 4.8) %. The chromatographic separation was performed at 35 °C and 16.0 MPa, and the best results were obtained at 4.8 % methanol concentration.²

In this way, the phase behavior of mitotane in supercritical CO₂ plus a cosolvent is an important information needed to develop separation process that employ the SFC technique. In this sense, we recently published experimental solubility data of mitotane in compressed and/or supercritical CO₂.³ The phase equilibrium data were determined within a temperature range from (298.2 to 333.1) K and at pressures up to 22.0 MPa. The Peng–Robinson equation of state (PR-EoS) with classical combining and mixing rules, coupled to an equation for the solid mitotane fugacity, which uses the mitotane sublimation pressure as a reference state, were used to correlate the experimental data. Calculation results, obtained mainly within the ranges of conditions of the experimental data, showed a good agreement between experimental and calculated values.

Because of the size and polarity asymmetry of the mitotane + CO₂ system, this binary mixture presents a quite complex phase behavior. The correct modeling of this system, in wide ranges of conditions, is therefore a scientific challenge.

Recently, Rodriguez-Reartes et al.⁴ performed phase equilibrium calculations for highly asymmetric systems, such as the propane + *n*-eicosane and CO₂ + *n*-eicosane binary mixtures, using path-following methods for tracking entire solid–fluid (SF) and solid–fluid–fluid (SFF) equilibrium curves. In this way, the authors obtained complete SF lines and three-phase equilibrium lines in single runs. More details on the calculation of SFF lines have been recently provided by Rodriguez-Reartes et al.¹⁴ The PR-EoS was used for describing the fluid phases, together with an expression for the fugacity of the pure *n*-eicosane solid phase, with parameter values that reproduced the pure *n*-eicosane melting curve.¹⁴ The simple model proposed by the authors was able to represent, at least qualitatively, both asymmetric mixtures. Such a model¹⁴ has derivatives with respect to temperature that are not discontinuous at the triple point temperature of the heavy component. This is not the case for models such as the one used by Favareto et al.³

A recent repetition of part of the experiments of Favareto et al.³ led us to conclude that the phase transition type (either FF or SF) was misidentified in some cases in such previous work. Therefore, the objective here is to provide new and/or revised phase equilibrium data for the system mitotane + CO₂ and new phase equilibrium data for the system mitotane + CO₂ + ethanol.

Special Issue: Kenneth N. Marsh Festschrift

Received: February 7, 2011

Accepted: June 8, 2011

Published: June 29, 2011

Table 1. Experimental Solid–Fluid (SF) and Fluid–Fluid (FF) Transition Data for CO₂ (1) + Mitotane (2) Binary Mixtures

| <i>T</i> | <i>P</i> | σ | transition | <i>T</i> | <i>P</i> | σ | transition |
|------------------------------|----------|----------|------------|------------------------------|----------|----------|------------|
| K | MPa | MPa | type | K | MPa | MPa | type |
| $x_1 = 0.9993, x_2 = 0.0007$ | | | | $x_1 = 0.9976, x_2 = 0.0024$ | | | |
| 298 | 6.65 | 0.01 | SF | 313 | 16.33 | 0.02 | SF |
| 303 | 7.96 | 0.06 | SF | 323 | 18.23 | 0.02 | FF |
| 313 | 10.21 | 0.06 | SF | 333 | 20.03 | 0.02 | FF |
| 313 | 10.51 | 0.05 | FF | $x_1 = 0.9972, x_2 = 0.0028$ | | | |
| 323 | 12.65 | 0.09 | FF | 313 | 18.53 | 0.02 | SF |
| 333 | 14.58 | 0.01 | FF | 323 | 20.00 | 0.02 | FF |
| $x_1 = 0.9990, x_2 = 0.001$ | | | | 333 | 21.84 | 0.02 | FF |
| 303 | 8.13 | 0.04 | SF | | | | |
| 313 | 10.62 | 0.02 | SF | | | | |
| 323 | 12.55 | 0.02 | FF | | | | |
| 333 | 14.42 | 0.01 | FF | | | | |
| $x_1 = 0.9986, x_2 = 0.0014$ | | | | | | | |
| 298 | 9.51 | 0.10 | SF | | | | |
| 303 | 10.52 | 0.12 | SF | | | | |
| 313 | 12.19 | 0.04 | SF | | | | |
| 313 | 12.49 | 0.02 | FF | | | | |
| 323 | 14.85 | 0.03 | FF | | | | |
| 333 | 16.84 | 0.04 | FF | | | | |
| $x_1 = 0.9979, x_2 = 0.0021$ | | | | | | | |
| 313 | 14.57 | 0.07 | SF | | | | |
| 313 | 15.03 | 0.04 | FF | | | | |
| 323 | 16.92 | 0.05 | FF | | | | |
| 333 | 19.41 | 0.01 | FF | | | | |

Table 2. Binary Interaction Parameters for the PR-EoS¹⁰

| system | k_{ij} | l_{ij} |
|-----------------------------------|----------|----------|
| carbon dioxide (1) + mitotane (2) | 0.161 | 0.230 |

Table 3. Mitotane Constants for eq 1 in Appendix A

| | |
|--|------------------------|
| T_{tp}/K^a | 353.15 |
| P_{tp}/MPa^b | $2.7312 \cdot 10^{-5}$ |
| $\Delta v^{S-L}/(m^3 \cdot K^{-1} \cdot mol^{-1})$ | -0.11640 |
| C_1/MPa | -1596.941 |
| C_2/MPa | 115214.836 |
| C_3/MPa | -134857.377 |

^aTaken from ref 3. ^b P_{tp} = PR-EoS¹⁰ pure compound vapor–liquid equilibrium pressure at the triple point temperature, T_{tp} .

work by eq 1 of Appendix A. The values, used in this work, for the pure mitotane constants required for evaluating the variable U of such equation are reported in Table 3, and their meaning is explained in Appendix A and in Table 3. We obtained the pure mitotane parameters C_1 , C_2 , C_3 , and Δv^{S-L} by fitting all the SF equilibrium experimental data reported in Table 1.

The set of equations for phase equilibrium calculations arises from imposing the classical necessary conditions: equal

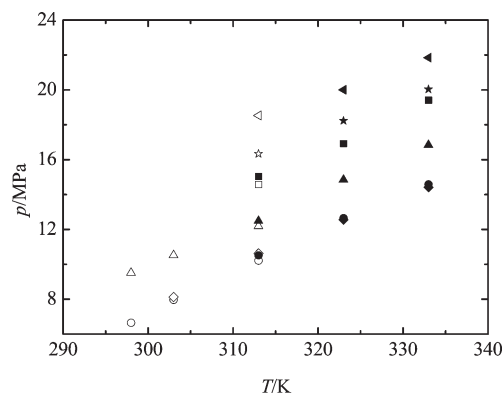


Figure 2. Experimental phase equilibrium data for CO₂ (1) + mitotane (2) mixtures obtained at global CO₂ concentrations $x_1 =$ left-pointing triangle, 0.9993; ☆, 0.9990; □, 0.9986; △, 0.9979; ▽, 0.9976; and ○, 0.9972. For each isopleth, SF and FF transitions are indicated by empty and full symbols, respectively.

temperature, pressure, and component fugacities in all phases. With regard to the calculation algorithms, we used numerical continuation methods for all phase equilibrium computations.

4. RESULTS AND DISCUSSION

4.1. Experimental Results. Table 1 presents the experimental data of phase transitions for the CO₂ (1) + mitotane (2) systems obtained at the global CO₂ mole fractions $x_1 = 0.9993$, 0.9990, 0.9986, 0.9979, 0.9976, and 0.9972. The difference between the data that Table 1 reports and the data by Favareto et al.³ lies, on one hand, on the corrected identification of the phase transition type for 10 data points, and, on the other hand, in the appearance, in Table 1, of eight new data points obtained in the present work (four of them correspond to $x_1 = 0.9990$). The correct identification of the phase transitions could be achieved because the experimental apparatus used in the present work permits a better visualization of the phase transitions than the one used by Favareto et al.³

In each isopleth, we observe SF and FF transitions. The data shown in Table 1 are plotted in the Figure 2 for better visualization and understanding of phase behavior of the system. From this figure we observe that all isopleths present SF transition segments at lower pressures and FF transitions at higher pressures. For all points in Table 1, the system is a homogeneous fluid at a pressure greater than the reported pressure, and it is a heterogeneous system otherwise.

To obtain the phase transition data for ternary mixtures of CO₂ (1) + ethanol (2) + mitotane (3), two solutions with different concentrations of mitotane in ethanol were prepared: 0.04 mol and 0.40 mol of mitotane per kg of ethanol. The solution concentration uncertainty was lower than $0.01 \text{ mol} \cdot \text{kg}^{-1}$. Tables 4 and 5 present results of ternary CO₂ (1) + ethanol (2) + mitotane (3) mixtures at two mitotane concentrations. In Table 4, the experimental data refer to vapor–liquid transitions at mitotane concentration of $0.04 \text{ mol} \cdot \text{kg}^{-1}$, where we identify vapor–liquid bubble point (BP) and dew point (DP) transitions. Table 5 presents the vapor–liquid transitions for mitotane concentration of $0.40 \text{ mol} \cdot \text{kg}^{-1}$. Again, bubble point (BP) and dew point (DP) transitions were identified. For all points in Tables 4 and 5, the system is a homogeneous fluid at a pressure greater than the reported pressure, and it is a heterogeneous FF system otherwise.

Table 4. Experimental Vapor–Liquid Transition Data for CO₂ (1) + Ethanol (2) + Mitotane (3) Ternary Mixtures at 0.04 mol·kg⁻¹ Mitotane Concentration in Ethanol (CO₂-Free Basis)

| <i>T</i> | <i>P</i> | σ | transition type | <i>T</i> | <i>P</i> | σ | transition type |
|--------------------------------|----------|----------|--------------------|--------------------------------|----------|----------|--------------------|
| K | MPa | MPa | | K | MPa | MPa | |
| <i>x</i> ₁ = 0.2085 | | | | <i>x</i> ₁ = 0.7092 | | | |
| 303 | 3.44 | 0.01 | BP | 303 | 5.96 | 0.01 | BP |
| 313 | 3.98 | 0.01 | BP | 313 | 7.24 | 0.01 | BP |
| 323 | 4.53 | 0.02 | BP | 323 | 8.50 | 0.01 | BP |
| 333 | 5.01 | 0.01 | BP | 333 | 9.84 | 0.01 | BP |
| <i>x</i> ₁ = 0.3203 | | | | <i>x</i> ₁ = 0.8072 | | | |
| 303 | 4.61 | 0.01 | BP | 303 | 6.18 | 0.01 | BP |
| 313 | 5.36 | 0.01 | BP | 313 | 7.49 | 0.01 | BP |
| 323 | 6.11 | 0.01 | BP | 323 | 8.82 | 0.05 | BP |
| 333 | 6.91 | 0.03 | BP | 333 | 10.16 | 0.01 | BP |
| <i>x</i> ₁ = 0.4104 | | | | <i>x</i> ₁ = 0.8653 | | | |
| 303 | 5.18 | 0.01 | BP | 303 | 6.16 | 0.01 | BP |
| 313 | 6.16 | 0.03 | BP | 313 | 7.52 | 0.01 | BP |
| 323 | 7.06 | 0.01 | BP | 323 | 8.95 | 0.03 | BP |
| 333 | 8.15 | 0.03 | BP | 333 | 10.28 | 0.01 | BP |
| <i>x</i> ₁ = 0.5015 | | | | <i>x</i> ₁ = 0.9232 | | | |
| 303 | 5.54 | 0.01 | BP | 303 | 6.18 | 0.01 | BP |
| 313 | 6.62 | 0.03 | BP | 313 | 7.46 | 0.03 | BP |
| 323 | 7.70 | 0.02 | BP | 323 | 8.85 | 0.01 | BP |
| 333 | 8.82 | 0.01 | BP | 333 | 10.10 | 0.03 | DP |
| <i>x</i> ₁ = 0.6011 | | | | <i>x</i> ₁ = 0.9595 | | | |
| 303 | 5.98 | 0.01 | BP | 303 | 6.33 | 0.02 | BP |
| 313 | 7.17 | 0.01 | BP | 313 | 7.66 | 0.02 | BP |
| 323 | 8.38 | 0.02 | BP | 323 | 8.73 | 0.03 | BP |
| 333 | 9.73 | 0.01 | BP | 333 | - | - | - |

Figure 3 provides a comparison (*p*–*x* diagram) between experimental VLE (vapor–liquid equilibrium) data obtained here for the ternary CO₂ (1) + ethanol (2) + mitotane (3) mixture at a concentration of mitotane of 0.04 mol·kg⁻¹ with binary data of CO₂ (1) + ethanol (2) (without mitotane) from the literature at (303 and 333) K.^{11,12} Figure 4 presents a similar comparison, but now the ternary mixture has a mitotane concentration of 0.40 mol·kg⁻¹.

Figure 3 shows that the low concentration of mitotane does not lead to significant changes in the transition pressures when the ternary system is compared to the corresponding binary system (without mitotane). However, Figure 4 shows that a higher concentration of mitotane leads to important changes in equilibrium conditions. For the concentration of 0.40 mol·kg⁻¹, there are large differences between the ternary experimental data measured here and the binary data from the literature, mainly in the region of lower concentration of CO₂.

In this work, we made no attempt to model the vapor–liquid equilibrium of the system CO₂ (1) + ethanol (2) + mitotane (3).

4.2. Modeling Results. In Figure 5f we present a phase envelope, including both SF and FF transitions, for the CO₂ (1) + mitotane (2) mixture, calculated using the PR-EoS and

Table 5. Experimental Vapor–Liquid Transition Data for CO₂ (1) + Ethanol (2) + Mitotane (3) Ternary Mixtures at 0.40 mol·kg⁻¹ Mitotane Concentration in Ethanol (CO₂-Free Basis)

| <i>T</i> | <i>P</i> | σ | transition type | <i>T</i> | <i>P</i> | σ | transition type |
|--------------------------------|----------|----------|--------------------|--------------------------------|----------|----------|--------------------|
| K | MPa | MPa | | K | MPa | MPa | |
| <i>x</i> ₁ = 0.2690 | | | | <i>x</i> ₁ = 0.6602 | | | |
| 303 | 5.04 | 0.01 | BP | 303 | 5.96 | 0.01 | BP |
| 313 | 5.77 | 0.01 | BP | 313 | 7.16 | 0.02 | BP |
| 323 | 6.57 | 0.02 | BP | 323 | 8.61 | 0.01 | BP |
| 333 | 7.32 | 0.02 | BP | 333 | 10.06 | 0.03 | BP |
| <i>x</i> ₁ = 0.3615 | | | | <i>x</i> ₁ = 0.7588 | | | |
| 303 | 5.79 | 0.01 | BP | 303 | 5.99 | 0.01 | BP |
| 313 | 7.03 | 0.02 | BP | 313 | 7.31 | 0.02 | BP |
| 323 | 8.50 | 0.02 | BP | 323 | 8.82 | 0.02 | BP |
| 333 | 9.77 | 0.02 | BP | 333 | 10.27 | 0.01 | BP |
| <i>x</i> ₁ = 0.4611 | | | | <i>x</i> ₁ = 0.8363 | | | |
| 303 | 5.75 | 0.01 | BP | 303 | 6.11 | 0.01 | BP |
| 313 | 7.10 | 0.01 | BP | 313 | 7.53 | 0.01 | BP |
| 323 | 8.60 | 0.01 | BP | 323 | 8.84 | 0.01 | BP |
| 333 | 10.05 | 0.01 | BP | 333 | 10.36 | 0.01 | BP |
| <i>x</i> ₁ = 0.5618 | | | | <i>x</i> ₁ = 0.8656 | | | |
| 303 | 5.85 | 0.01 | BP | 303 | 6.33 | 0.02 | BP |
| 313 | 7.25 | 0.02 | BP | 313 | 7.60 | 0.01 | BP |
| 323 | 8.72 | 0.03 | BP | 323 | 9.01 | 0.03 | BP |
| 333 | 10.16 | 0.01 | BP | 333 | 10.41 | 0.04 | DP |

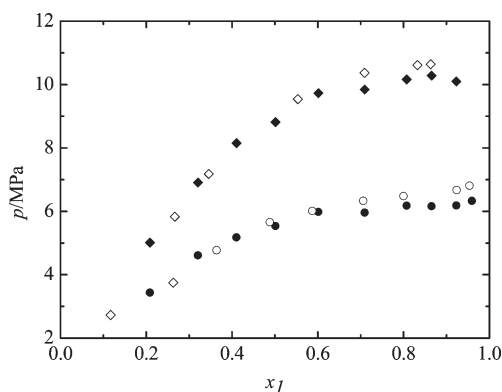


Figure 3. *P*–*x* VLE diagram for the CO₂ (1) + ethanol (2) + mitotane (3) mixture at a mitotane concentration in ethanol of 0.04 mol·kg⁻¹. Full symbols are the ternary experimental data from this work: ◆, 303 K and ●, 333 K. Empty symbols are the experimental data from the literature for the binary system CO₂ (1) + ethanol (2): ◇, 303 K¹² and ○, 333 K.¹¹

eq 1, at 0.0028 mitotane mole fraction, that is, at the highest mitotane concentration shown in Table 1. At high pressure and low temperature, we observe a SF transition segment that goes to low pressure and intersects a liquid–vapor equilibrium line (dew point) at about 16.7 MPa. This point corresponds to a three-phase (solid–liquid–vapor) equilibrium at 0.0028 mitotane mole fraction. The liquid–vapor (LV) segment (dew line) that

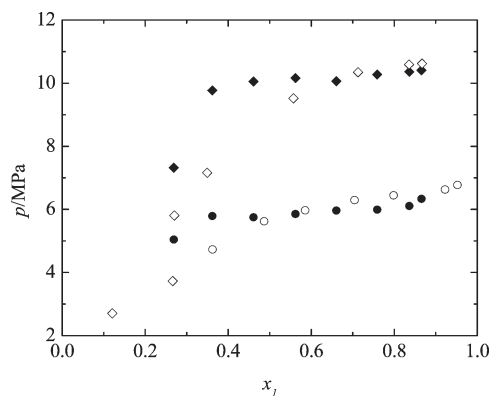


Figure 4. P - x VLE diagram for the CO_2 (1) + ethanol (2) + mitotane (2) mixture at a mitotane concentration in ethanol of $0.40 \text{ mol} \cdot \text{kg}^{-1}$. Full symbols are the ternary experimental data from this work: \blacklozenge , 303 K and \bullet , 333 K. Empty symbols are the experimental data from the literature for the binary system CO_2 (1) + ethanol (2): \diamond , 303 K¹² and \circ , 333 K.¹¹

originates at such a three-phase point goes through a maximum in pressure and then through a maximum in temperature. At very low pressure, the LV transition line intersects another SF transition segment that is hard to see in Figure 5f due to the linear scale in pressure. This SF segment is better visualized in Figure 6f, where a logarithmic scale for pressure is used. In this figure we observe clearly the second three phase solid–liquid–vapor point at about 0.01 MPa. Notice that the abbreviation FF located inside the heterogeneous region of, for example, Figure 5f, indicates a point where the phase condition is a FF equilibrium. Similarly, the abbreviation SF is written at a point where the phase condition is a SF equilibrium.

Notice that the PR-EoS and eq 1 capture the qualitative behavior observed experimentally in the laboratory. For example, at the temperature and pressure conditions of point A in Figure 5f, the model gives a homogeneous fluid state. If we decrease the pressure at constant temperature, that is, at 313 K, from point A to point C, we reach a heterogeneous SF condition at point C. At such temperature, the limit between the homogeneous and heterogeneous states is located at point B, where the fluid phase is saturated in mitotane (at equilibrium with a pure mitotane solid phase).

From Figure 6f, we notice that the model (PR-EoS and eq 1) predicts a minimum in temperature for the high-pressure SF line at 0.0028 mitotane mole fraction. Thus, for this isopleth composition, at any temperature lower than about 304 K (which is approximately the temperature of the minimum), it would not be possible to observe a (dense) homogeneous phase even at very high pressure conditions (at least up to 200 MPa which is the maximum pressure of the actual calculations carried out for generating Figures 5f and 6f).

In Figure 5f and according to the model, at about 20.0 MPa and 500 K, the system is a homogeneous fluid (made of only one phase). Then, by decreasing the temperature while keeping the pressure constant at 20.0 MPa, a second fluid phase appears when the dew line is crossed for the first time. The system presents two phases (FF system). The two coexisting fluid phases remain within a large temperature range, until the FF line (dew line) is intersected again. A further decrease in temperature takes the system back to a homogeneous fluid phase condition. By decreasing the temperature even more, the SF line is intersected,

and a solid phase, pure mitotane, appears. This SF coexistence remains even at very low temperatures.

The negative slope of the high-pressure SF line in Figure 5f, predicted by the model [PR-EoS and eq 1], corresponds to a retrograde solidification with respect to pressure, which is characterized by the disappearance of a solid phase with the increase in pressure, as it happens when going from point C to point A (through the intersection point B) in Figure 5f. However, according to the model, if the pressure is further increased from point A, at constant temperature, a new intersection point is reached (see Figure 6f), and a solid phase, pure mitotane, reappears. Thus, for the model [which predicts a change in slope for the high pressure SF line (Figure 6f)], the normal behavior is recovered at a high enough pressure.

Figure 5a shows a phase envelope obtained from the (PR-EoS and eq 1) model (lines) and also shows experimental data (points) for the CO_2 (1) + mitotane (2) mixture at 0.0007 mitotane mole fraction (the lowest mitotane concentration in Table 1). This figure presents, for the model, a high-pressure SF equilibrium segment (S_I) that exists in a narrow temperature range. A bubble point segment connects the SF segment S_I with a second SF segment S_{II} , which has a positive slope and has a wider temperature range than S_I . The S_{II} SF segment intersects a dew point line at higher temperatures. The calculated dew and S_{II} segments are consistent with the experimental data obtained in our laboratory (circles shown in Figures 5a and 6a). Indeed, we looked for such consistency while fitting the parameters of the model. Similar to the previous system shown in Figures 5f and 6f, another SF equilibrium segment (S_{III}) appears at very low pressures. Comparing the calculated dew and S_{II} segments with the FF and SF experimental data shown in Figure 5a, we conclude that, clearly, the model (PR-EoS and eq 1) correlates very well the SF data and provides a fair description of the FF data. However, the model over predicts both the temperature and the pressure of the intersection point of the (SF) S_{II} and dew (FF) segments, that is, of the three-phase point.

In Figure 5a, the calculation results obtained with the model suggest that there is a pressure range within which it is possible to reach, at constant pressure, SF transitions from an initial homogeneous fluid state, either by increasing the temperature (retrograde behavior) or by decreasing the temperature (normal behavior). Of both phenomena, the retrograde behavior is confirmed by our experimental data (filled circles) in Figure 5a. Consider for example a constant pressure of 8.0 MPa. From an initial SF condition, that is, a point at 8.0 MPa located just to the right of the S_{II} segment, a decrease in temperature takes the system to a single phase region after the SF S_{II} segment is crossed (retrograde melting at constant pressure, RMCP). A further decrease in temperature takes the system again to a SF condition at a low enough temperature (normal solidification at constant pressure) after the SF S_I segment is intersected. This complex behavior is due to the SF line S_{II} that exists at intermediate temperatures. It should be clear that for a system showing RMCP it is possible to melt a solid phase by decreasing the temperature. The phenomenon of retrograde melting at constant pressure could be attributed to the nonlinear decrease of the solvent density (CO_2), and the corresponding behavior of its dielectric constant (reduction of solvent power), when temperature is raised under conditions close to the critical conditions of the solvent (carbon dioxide). Figure 6a shows the phase diagram of Figure 5a but in logarithmic scale for the pressure, for better visualization of the phase behavior in a larger pressure range. We notice that the SF transition line S_I presents a minimum

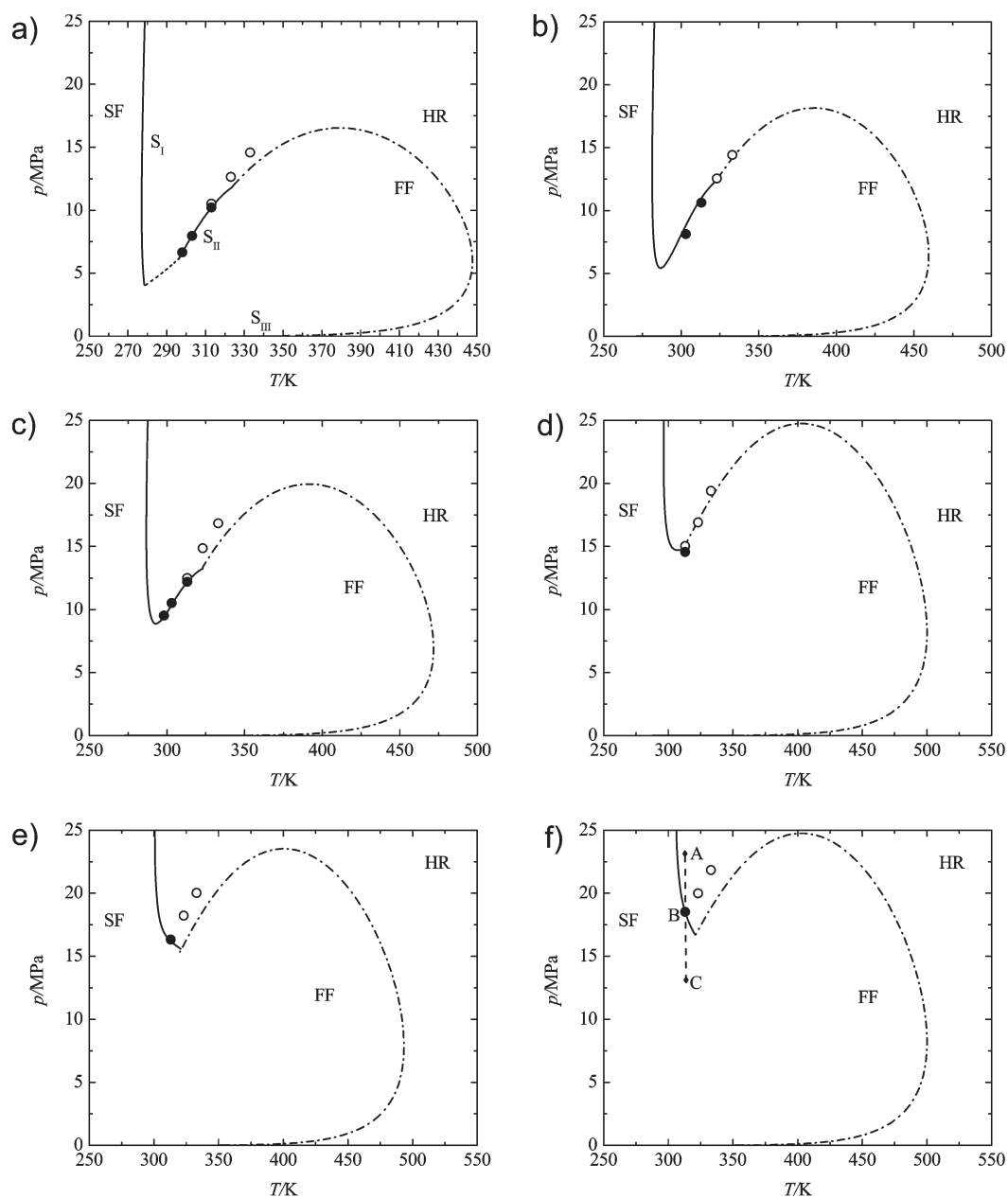


Figure 5. Phase envelopes for the CO₂ (1) + mitotane (2) mixture. Mitotane mole fraction values: a: 0.0007, b: 0.001, c: 0.0014, d: 0.0021, e: 0.0024, f: 0.0028. ○, experimental FF equilibrium data; ●, experimental SF equilibrium data (experimental data are shown in Table 1). Phase equilibria calculated using the PR-EoS and eq 1 of Appendix A: solid line, SF; dashed line, bubble points (FF); dot–dashed line, dew points (FF). Note for part f: At point A, the system is an homogeneous fluid. At points B and C, the system has a heterogeneous SF state. HR: homogeneous region; FF: fluid–fluid region and SF: solid–fluid region.

in temperature indicative of mitotane retrograde crystallization at constant temperature (RCCT). We have not performed experiments under the conditions of the S_I SF segment. Thus, the RCCT at low temperature is a prediction by the model (PR-EoS and eq 1) that would have to be confirmed through additional experiments. The SF segments S_I and S_{III} predicted by the model conform to the common sense expectation that at a low enough temperature a solid phase must be present in the system. This must happen even in the case of existence of RMCP at an intermediate temperature range (segment S_{II}).

Notice that the segment S_{II} (Figure 5a) presents not only RMCP but also RCCT, since an increase in pressure at constant

temperature takes the system from the SF state to the homogeneous fluid state if the segment S_{II} is crossed. It is clear that for segment S_{II} the experimental data support the conclusion that the system CO₂ + mitotane presents, at intermediate temperatures, retrograde melting (or retrograde crystallization) both at constant temperature and at constant pressure.

Figures 5b and 6b show the phase envelope obtained from the model (PR-EoS and eq 1, lines) and also show experimental data (points) for the CO₂ (1) + mitotane (2) mixture at 0.001 mitotane mole fraction. For this isopleth, a bubble point line at intermediate temperatures (such as the one shown in Figures 5a and 6a for a lower mitotane concentration) does not exist.

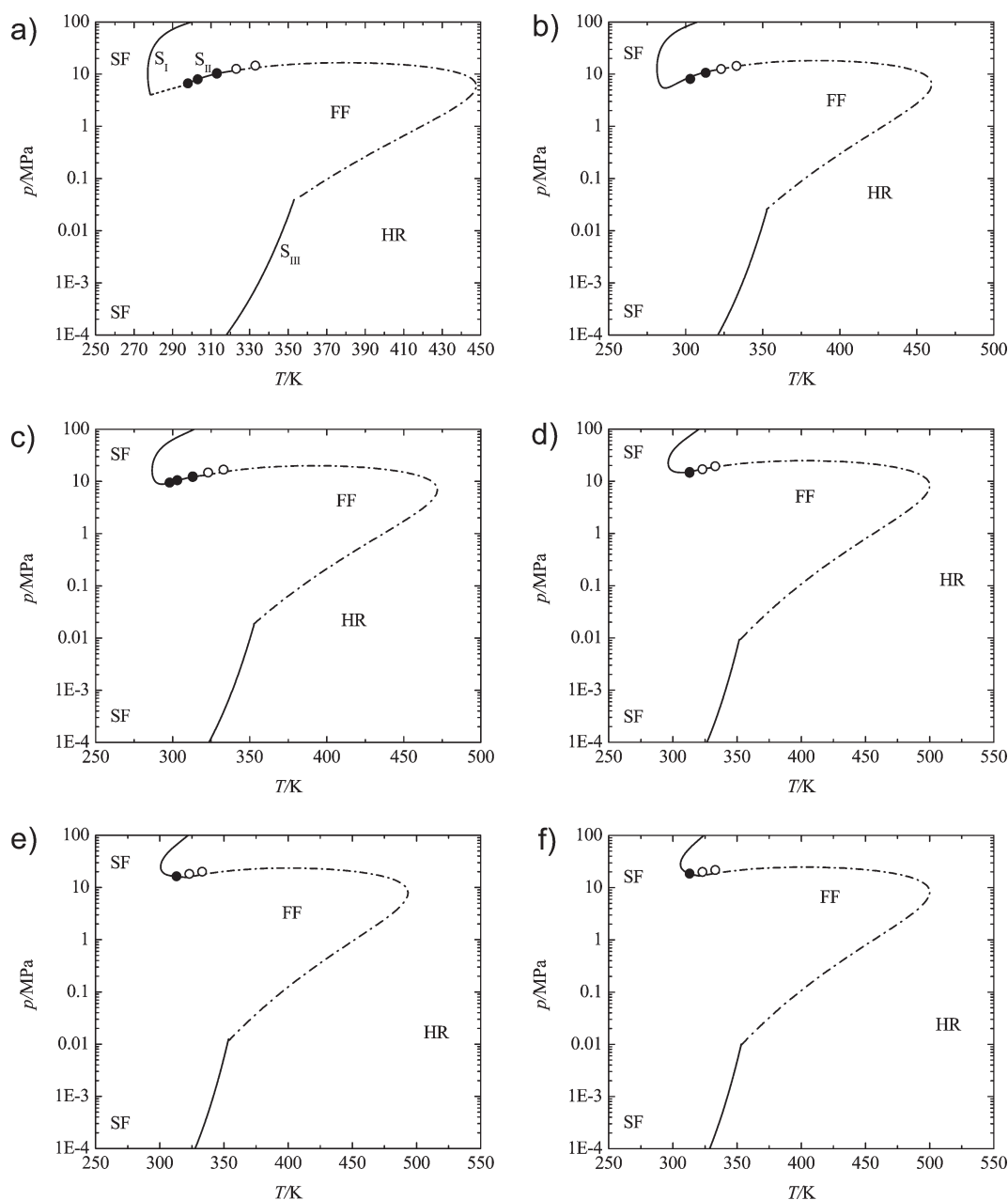


Figure 6. Phase envelopes, with pressure in log scale, for the CO₂ (1) + mitotane (2) mixture. Mitotane mole fraction values: a: 0.0007, b: 0.001, c: 0.0014, d: 0.0021, e: 0.0024, f: 0.0028. ○, experimental FF equilibrium data; ●, experimental SF equilibrium data (experimental data are shown in Table 1). Phase equilibria calculated using the PR-EoS and eq 1 of Appendix A: solid line, SF; dashed line, bubble points (FF); dot–dashed line, dew points (FF). HR: homogeneous region; FF: fluid–fluid region, and SF: solid–fluid region.

However, the retrograde melting at constant pressure (RMCP) behavior remains. A similar phase diagram is observed for 0.0014 mitotane mole fraction (shown in Figures 5c and 6c).

Figures 5d and 6d and 5e and 6e show phase diagrams obtained from the model (lines) and also show experimental data (points) for the CO₂ (1) + mitotane (2) mixture at 0.0021 and 0.0024 mitotane mole fraction, respectively. These phase diagrams are similar to that of 0.0028 mitotane mole fraction shown in Figures 5f and 6f. According to the model, for these isopleth conditions the mixtures present no bubble point line at intermediate temperatures, neither retrograde melting at constant pressure.

Even though the PR-EoS with classical combining and mixing rules coupled to eq 1 of Appendix A describes reasonably well the

phase diagrams presented here, it might be possible to improve the model performance by using a nonclassical mixing rule. The need for more complex mixing rules (MRs), such as the Wong–Sandler²⁴ MR, or the cubic mixing rules,^{13,22} is typically expected for highly asymmetric binary systems as mitotane–CO₂ studied here.

It is clear that we have adjusted six parameters for the system CO₂ + mitotane, that is, parameters k_{ij} , l_{ij} , C1, C2, C3, and Δv^{S-L} . However, all of these parameters were not fitted simultaneously. Parameters k_{ij} and l_{ij} were fitted first, using only FF equilibrium information. Parameters C1, C2, C3, and Δv^{S-L} were fit next, using only SF equilibrium data. During this second step, parameters k_{ij} and l_{ij} remained fixed and set at the values of

Table 2. Notice that although in this work we obtained parameters k_{ij} , l_{ij} , C1, C2, C3, and Δv^{S-L} from binary information, strictly, only parameters k_{ij} , l_{ij} are binary, while parameters C1, C2, C3, and Δv^{S-L} are pure compound parameters.

If pure mitotane solid–liquid equilibrium data, in a wide enough pressure range, had been available, it would have been possible to obtain the constants C1, C2, and C3 from such pure mitotane experimental data, as done for *n*-eicosane by Rodriguez-Reartes et al.^{4,14} Next, parameter Δv^{S-L} , that is, the only remaining degree of freedom, would have been fitted from mixture SF equilibrium data.^{4,14} The (indeed different) approach we chose in this work to fit the model parameters was defined on the basis of the available experimental data. The values for the constants C1, C2, and C3 reported in Table 3 are such that the calculated pure mitotane liquid–solid equilibrium curve (not shown in this article) has a positive slope at least up to 200 MPa.

Notice that the computation of constants C1, C2, and C3 from pure compound solid–liquid equilibrium data is analogous to imposing the reproduction of the pure compound vapor–liquid equilibrium curve for models of the equation of state type, designed for describing equilibria between fluid phases.

The alternative approach of using mixing rules, within the PR-EoS, more flexible with regard to composition and temperature,²² that is, the use of a number of binary interaction parameters greater than two, when reproducing FF equilibrium data with the model, might have reduced the need for nonzero parameters (C1, C2, C3, and Δv^{S-L}) in eq 1 of Appendix A, when reproducing the SF equilibrium data.

Models which, because of their theoretical basis, are often regarded as more advanced than the one used here, for example, the PC-SAFT²³ EOS for describing fluid phases, may lead to inconsistent behavior due to the appearance of liquid–liquid coexistence curves for pure fluids, that is, of a phenomenon that has never been experimentally observed.²³

5. CONCLUSION

Phase transition measurements for binary mixtures of CO₂ (1) + mitotane (2) and ternary mixtures of CO₂ (1) + ethanol (2) + mitotane (3) are provided here.

For binary mixtures of CO₂ (1) + mitotane (2) we provide experimental data on SF and FF transitions for six isopleths (mitotane mole fractions of 0.0007, 0.001, 0.0014, 0.0021, 0.0024, and 0.0028).

The experimental data for CO₂ (1) + mitotane (2) at 0.0007, 0.001, and 0.0014 mitotane mole fraction show retrograde melting (or retrograde crystallization) at constant pressure, and also at constant temperature, that is, they show that the solid phase is melted either by decreasing the temperature at constant pressure or by increasing the pressure at constant temperature.

This behavior is properly captured by a model built by combining the PR-EoS (with classical combining and mixing rules) with an equation that describes the fugacity of pure compounds in solid state, that is, eq 1 of Appendix A. The model also predicts, for all isopleths studied here, the occurrence, at low temperatures, of retrograde mitotane melting at constant temperature, which corresponds to the existence, in the low temperature range, of a point of minimum temperature in the predicted SF equilibrium line. The existence of this phenomenon, at low temperatures, for the CO₂ (1) + mitotane (2) system should be regarded, for the time being, as a presumption. Additional experiments should be performed to confirm or reject

this expectation. Gregorowicz¹⁵ has analyzed the criteria for the existence of retrograde melting at constant temperature.

The numerical continuation methods used in the calculations were essential to track the highly nonlinear SF equilibrium curves computed with the model.

The calculated isopleths have a temperature range wider than the temperature range studied experimentally. In spite of the potentially important errors that, from the quantitative point of view, such extrapolations may carry, the calculation results obtained in the present work, over wide ranges of conditions, are useful to enhance our understanding of the possible qualitative, highly nonideal, behavior of the present and related systems.

Here we also provide liquid–vapor equilibrium data of ternary mixtures of CO₂ (1) + ethanol (2) + mitotane (3) for two concentrations of mitotane in ethanol: 0.04 mol and 0.40 mol of mitotane per kg of ethanol. A low concentration of mitotane does not lead to significant changes in the transition pressures with respect to the mitotane-free binary system. In contrast, a higher concentration of mitotane produces important changes in the equilibrium conditions.

■ APPENDIX A: THERMODYNAMIC MODEL

The model used in this work for describing phase equilibria involving fluid and solid phases is the same than the model used in previous works.^{4,14} To describe the fluid state of a binary mixture of a light component (labeled “1”) and a heavy component (labeled “2”), we use a pressure-explicit equation of state (EOS), that is, a relationship between the absolute pressure (P), the absolute temperature (T), the mixture molar volume (v), and the mixture composition z_2 , where z_2 is the mole fraction of component “2”. We represent such a relationship as $P = h_{PVT}(T, z_2, v)$, where the form of function h_{PVT} corresponds to the adopted EOS, for example, to the Peng–Robinson (PR)¹⁰ EOS, that is, the EOS that we used in this work. The h_{PVT} function imposes the expression for the fugacity of component “ i ” in the fluid mixture (\hat{f}_i). Thus, \hat{f}_i depends on the same variables than function h_{PVT} , that is, $\hat{f}_i = \hat{f}_i(T, z_2, v)$. Indeed, this last functional relationship also corresponds in this work to the PR-EoS.¹⁰

Due to the high asymmetry of the binary system that we consider in this work, we assume that a given solid phase is made of only the pure heavy component (component “2”, i.e., mitotane in this work). Thus, for performing equilibrium calculations, we need an equation relating the fugacity of the pure component “2” in solid state to the absolute pressure (P) and to the absolute temperature (T) of the system. We define, mathematically, the fugacity of the pure heavy component “2” in solid state at T and P , that is, $f_2^S(T, P, v_o)$, (where v_o actually depends on T and P) as follows:

$$f_2^S(T, P, v_o) = \hat{f}_2(T, 1, v_o) \exp(U) \quad (1)$$

In eq 1, v_o is the molar volume of the pure heavy component (component “2”), in (subcooled hypothetical) liquid state, at T and P . Such pure liquid has a fugacity $\hat{f}_2(T, 1, v_o)$ (first factor within the right-hand side of eq 1). Notice that the expression $\hat{f}_2(T, 1, v_o)$ simply states that the function $\hat{f}_i = \hat{f}_i(T, 1, v_o)$, with subscript “ i ” set equal to “2”, is evaluated at $z_2 = 1$ and at $v = v_o$, that is, that the computed fugacity corresponds to a liquid made of the pure heavy compound, having such pure liquid a molar volume equal to v_o . Both, v_o and $\hat{f}_2(T, 1, v_o)$ are given in this work by the PR-EoS.¹⁰ The exponential factor in eq 1 relates

(through eq 1) the hypothetical liquid state with the solid state for a pure substance at given temperature and pressure. The variable U , which depends on T and P , is defined as follows:

$$U = \frac{\Delta v^{S-L}}{RT_{tp}} \left[C_1 \left(1 - \frac{T_{tp}}{T} \right) + C_2 \left(\frac{T_{tp}}{T} - 1 + \ln \left(\frac{T}{T_{tp}} \right) \right) + C_3 \left(\frac{T}{2T_{tp}} - 1 + \frac{T_{tp}}{2T} \right) + \frac{T_{tp}}{T} (P - P_{tp}) \right] \quad (2)$$

In eq 2, the constants T_{tp} , P_{tp} , Δv^{S-L} , C_1 , C_2 , and C_3 (see Table 3) correspond to the pure heavy component (component "2"). Δv^{S-L} is the solid–liquid molar volume difference ($v_{\text{solid}} - v_{\text{liquid}}$). The constants C_1 , C_2 , and C_3 characterize the pure heavy component solid–liquid equilibrium curve (P vs T melting curve). R is the universal gas constant.

For computing $f_2^S(T, P, v_o)$ at set T and P , we would first calculate v_o from the adopted EoS [$P - h_{PVT}(T, 1, v_o) = 0$], next we would compute $\hat{f}_2(T, 1, v_o)$, then U from eq 2, and, finally, plug the results into the right-hand side of eq 1, to obtain the value of $f_2^S(T, P, v_o)$. We stress that the phase type for $f_2^S(T, P, v_o)$ is "solid" while the phase type for $\hat{f}_2(T, 1, v_o)$ is "liquid", and that both fugacities correspond to the same T and P values.

The variable v_o , that is, a property of a pure liquid, appears as an argument for the fugacity of the pure solid [on the left-hand side of eq 1] because the fugacity of the pure solid is partially computed from the fugacity of the pure liquid, that is, from a liquid-state reference fugacity, being the temperature and pressure for such reference fugacity the same than the temperature and pressure of the solid.

The calculation of a binary phase equilibrium point requires solving the isofugacity condition for component "1" in all fluid phases and for component "2" in all fluid phases and in the solid phase (if present), after imposing the constraint of uniform pressure and uniform temperature throughout the heterogeneous system.

More details on the model used here were given by Rodriguez-Reartes et al.¹⁴

AUTHOR INFORMATION

Corresponding Author

*Phone: +55-21-25627650. Fax: +55-21-25627567. E-mail: tavares@eq.ufjf.br.

REFERENCES

- (1) Dias, R. M.; Santana, C. C. Transferência de Massa e Efeitos Termodinâmicos na Separação do Fármaco Mitotano por Cromatografia Líquida de Alta Eficiência (in portuguese). *Proceedings of IV Congresso Brasileiro de Termodinâmica Aplicada*, Recife, Brazil, 2008.
- (2) Antelo, F.; Santana, C. C.; Barreto, A. G., Jr.; Alves, T. L. M. Enantioseparation of Mitotane by Supercritical Fluid Chromatography on Kromasil Chi-Tbb at 160 bar. *Proceedings of II Iberoamerican Conference on Supercritical Fluids – PROSCIBA*, Natal-RN, Brazil, 2010.
- (3) Favareto, R.; Pereira, J. R. D.; Santana, C. C.; Madureira, E. H.; Cabral, V. F.; Tavares, F. W.; Cardozo-Filho, L. High-pressure phase diagram of the drug mitotane in compressed and/or supercritical CO₂. *J. Chem. Thermodyn.* **2010**, *42* (2), 286–290.
- (4) Rodriguez-Reartes, S. B.; Cismondi, M.; Franceschi, E.; Corazza, M. L.; Oliveira, J. V.; Zabaloy, M. S. High-pressure phase equilibria of systems carbon dioxide + n-eicosane and propane + n-eicosane. *J. Supercrit. Fluids* **2009**, *50* (3), 193–202.

- (5) Carvalho, J. R. N.; Corazza, M. L.; Cardozo-Filho, L.; Meireles, M. A. A. Phase Equilibrium for (Camphor + CO₂), (Camphor + Propane) and (Camphor + CO₂ + Propane). *J. Chem. Eng. Data* **2006**, *51* (3), 997–1000.

- (6) Favareto, R.; Cabral, V. F.; Corazza, M. L.; Cardozo-Filho, L. Vapor–liquid and solid–fluid equilibrium for progesterone + CO₂, progesterone + propane, and progesterone + n-butane systems at elevated pressures. *J. Supercrit. Fluids* **2008**, *45* (2), 161–170.

- (7) Souza, A. T.; Benazzi, T. L.; Grings, M. B.; Cabral, V. F.; Silva, E. A.; Cardozo Filho, L.; Antunes, O. A. C. Supercritical extraction process and phase equilibrium of Candeia (*Eremanthus erythropappus*) oil using supercritical carbon dioxide. *J. Supercrit. Fluids* **2008**, *47*, 182–187.

- (8) Favareto, R.; Fregadolli, P. H.; Cabral, V. F.; Antunes, O. A. C.; Cardozo-Filho, L. Phase Equilibria of Acrylonitrile and p-Bromobenzaldehyde in Carbon Dioxide. *J. Chem. Eng. Data* **2008**, *53* (5), 1080–1084.

- (9) Moura, L. S.; Favareto, R.; Leal, P. F.; Corazza, M. L.; Cardozo-Filho, L.; Meireles, M. A. A. Phase-Equilibrium Measurements for CO₂ + Pripricoa Extract at High Pressures. *J. Supercrit. Fluids* **2009**, *48*, 126–130.

- (10) Peng, D.-Y.; Robinson, D. B. A New Two-Constant Equation of State. *Ind. Eng. Chem. Fundam.* **1976**, *15* (1), 59–64.

- (11) Joung, S. N.; Yoo, C. W.; Shin, H. Y.; Kim, S. Y.; Yoo, K.-P.; Lee, C. S.; Huh, W. S. Measurements and correlation of high-pressure VLE of binary CO₂-alcohol systems (methanol, ethanol, 2-methoxyethanol and 2-ethoxyethanol). *Fluid Phase Equilib.* **2001**, *185*, 219–230.

- (12) Chiu, H.-Y.; Lee, M.-J.; Lin, H.-M. Vapor-Liquid phase boundaries of binary mixtures of carbon dioxide with ethanol and acetone. *J. Chem. Eng. Data* **2008**, *53*, 2393–2402.

- (13) Zabaloy, M. S. Cubic Mixing Rules. *Ind. Eng. Chem. Res.* **2008**, *47*, 5063–5079.

- (14) Rodriguez-Reartes, S. B.; Cismondi, M.; Zabaloy, M. S. Computation of solid–fluid–fluid equilibria for binary asymmetric mixtures in wide ranges of conditions. *J. Supercrit. Fluids* **2011**, *57*, 9–24.

- (15) Gregorowicz, J. Phase behaviour in the vicinity of the three-phase solid–liquid–vapour line in asymmetric nonpolar systems at high pressures. *Fluid Phase Equilib.* **2006**, *240*, 29–39.

- (16) Deiters, U. K.; Schneider, G. M. High Pressure Phase Equilibria: Experimental Methods. *Fluid Phase Equilib.* **1986**, *29*, 145–160.

- (17) Suppes, Q. J.; Mchugh, M. A. Phase Behavior of the Carbon Dioxide-Styrene System. *J. Chem. Eng. Data* **1989**, *34*, 310–312.

- (18) Christov, M.; Dohrn, R. High-Pressure Fluid Phase Equilibria: Experimental Methods and Systems Investigated (1988–1993). *Fluid Phase Equilib.* **1995**, *106*, 213–282.

- (19) Christov, M.; Dohrn, R. High-Pressure Fluid Phase Equilibria: Experimental Methods and Systems Investigated (1994–1999). *Fluid Phase Equilib.* **2002**, *202*, 153–218.

- (20) Ashour, I.; Hammam, H. Equilibrium Solubility of Pure Mono-, Di-, and Trilaurin in Supercritical Carbon Dioxide Experimental Measurements and Model Prediction. *J. Supercrit. Fluids* **1993**, *6*, 3–8.

- (21) DIPPR 801, *Evaluated Process Design Data*, Public Release in American Institute of Chemical Engineers, Design Institute for Physical Property Data; BYU-DIPPR, Thermophysical Properties Laboratory: Provo, UT, 2003.

- (22) Cismondi, M.; Mollerup, J. M.; Zabaloy, M. S. Equation of state modeling of the phase equilibria of asymmetric CO₂ + n-alkane binary systems using mixing rules cubic with respect to mole fraction. *J. Supercrit. Fluids* **2010**, *55*, 671–681.

- (23) Privat, R.; Gani, R.; Jaubert, J. N. Are safe results obtained when the PC-SAFT equation of state is applied to ordinary pure chemicals? *Fluid Phase Equilib.* **2010**, *295*, 76–92.

- (24) Wong, D. S. H.; Sandler, S. I. A theoretically correct mixing rule for cubic equations of state. *AIChE J.* **1992**, *38*, 671–680.